



Unified refined beam theory applied to the spectral finite element method for analysis of laminated composites

Hilton Marques S. Santana¹, Luís Philipe R. Almeida² and Fabio Carlos da Rocha³*

¹Department of Civil Engineering, Federal University of Sergipe, São Cristovão, Brazil

²Department of Civil Engineering, Federal University of Sergipe, São Cristovão, Brazil

³Federal University of Alagoas, Laboratory of Scientific Computing and Visualization Technology Center, Campus A. C. Simões, Macei&ocute;-AL, 57092-970, Brazil

Abstract

Due to the limitation that the classical beam theories have in representing transversal shear stress fields, new theories, called high order, have been emerging. In this work, the principal high order theories are unified in single kinematics and applied to the Equivalent Single Layer Theory. The governing equations and the boundary conditions for laminated beams are consistent variational obtained. From the equilibrium equations, the high order spectral finite element model was developed using the polynomial functions of Hermite and Lagrange, with interpolants in the zeros of Lobatto's polynomials. Finally, to demonstrate the finite element model's outstanding efficiency, numerical results (static and dynamic) are shown and compared with the elasticity theory solution.

Keywords: Laminated beams ESL theory Spectral Finite Element Method.

1. Introduction

In recent years, composite material beams have achieved great prominence in civil, aeronautical, naval, and mechanical engineering. This applicability of composite materials is due to the better mechanical properties of these materials, such as strength, stiffness, weight, and thermal conductivity. However, shear deformation's effects become more pronounced in composite structures due to the low transverse shear modules compared to longitudinal, when subjected to transverse loads. Two approaches to construction of beam theories are commonly found in the literature: only from the displacement field and others from both the displacement and stress fields, thus named mixed theories [1, 2].

Among the theories coming from a displacement field, we highlight the classical Euler-Bernoulli Theory (EBT), the First Shear-Deformation Theory (FSDT), or Timoshenko Theory, and the High Order shear Deformation Theories (HSDT). Initially, these theories were developed for isotropic beams and with only one layer; however, through the equivalent Single-Layer Theories (ESL), it is possible to extend such models to orthotropic and laminated beams [1, 3]. EBT developed in the 18th century is considered the simplest model, as it does not adopt deformation due to shear in its displacement field. The FSDT theory, developed at the beginning of the 20th century by Timoshenko [4], considers the constant field for shear deformation. However, FSDT does not admit the nullity of the shear stress at the upper and lower edges of the beam, causing the need to use correction factors for better efficiency of results. From the middle of the 20th century, High Order Theories emerged with the primary objective of overcoming the existing limitation in the FSDT.

* Corresponding author. Tel.: +55-079-3196-6700; e-mail: fcrocha@ufs.br

The high-order models (HSDT) describe the beam displacement field using polynomial, trigonometric, exponential, and hyperbolic functions [5-12] that guarantee the possibility of nulling the shear stress at the upper and lower edges of the beam. Sayyad and Ghugal [13] present some high-order theories and conclude that approaches that consider parabolic variation for the transverse shear stress do not need the shear correction factor. Moreover, they state that models with polynomial, trigonometric, hyperbolic, and exponential functions in the in-plane displacement fields give excellent values for displacements and stresses. Finally, they state that the modular ratio increase provides lower values for axial and transverse displacements and higher values for stresses.

It is also important to highlight that the Equivalent Layer Theories (ESL) provide accurate transverse displacement, free vibration, and buckling and are not very precise for the stress field [14, 15]. This deficiency occurs due to the adoption of a Class C1 displacement field that provides a continuous stress field, in which they should be discontinuous when there are different values of the transversal shear module for adjacent layers. One way to get around this inconvenience is to obtain the shear stress field from the elasticity equilibrium equations [15].

To solve varying complexity problems, the computational implementation of beam theories using the Finite Element Method is typical. In this sense, Heyliger and Reddy[16] present a finite element to describe the static and dynamic behavior of beams, with a rectangular cross-section, using Reddy's variational consistent approach [5]. The model developed in [16] was compared with the elasticity theory's analytical solutions and achieved satisfactory results.

One way to accelerate the convergence of results in the FEM-models is to increase the interpolation order with the interpolating points (nodal points) at the positions of the zeros of the orthogonal polynomials, thus constituting the High Order Spectral Finite Element Method (SFEM). It is common in solid mechanics to use this method for wave propagation problems [17, 18]. However, its application in static problems is still little explored due to increased mathematical complexity and computational cost [19]. Thus, the present work's objective is to investigate the advantages of implementing high order beam (ESL) theories, via SFEM with any order approximation. For this, the general finite element model was developed by applying high-order interpolation to the nodal base formed by the zeros of Lobatto's orthogonal polynomials. Finally, the static and free vibration analysis results are compared with the results obtained in Pagano [20] and Giunta et al. [21].

2. Governing equations

2.1. Kinematics

Consider a beam of thickness equal to h composed of N orthotropic layers with the principal material coordinates (x_1^k, x_x^k, x_3^k) of the k th lamina oriented at an angle θ_k about the x coordinate. The k th layer is located between points $z = z_k$ and $z = z_{k+1}$ in the thickness (see Figure 1).

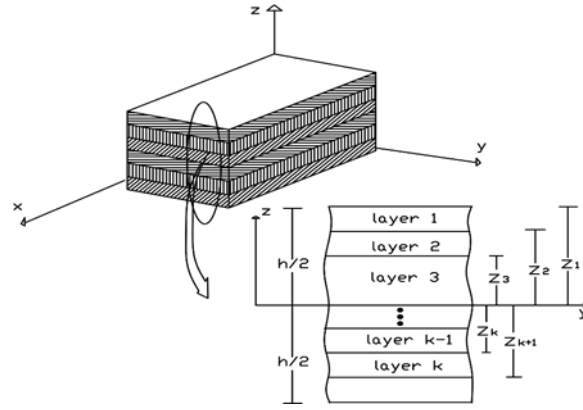


Figure 1. Geometry description of a laminated composite beam.

The unified displacement field is shown in Eq.(1) [13] to cover several refined theories'

$$\text{kinematics: } \begin{cases} u(x, z, t) = -z \frac{\partial w}{\partial x} + f(z)\phi \\ w(x, z, t) = w(x, t) \end{cases} \quad (1)$$

where $u(x, z, t)$, $w(x, t)$, and $\phi(x, t)$ represent, respectively, axial displacement, transversal displacement, and the cross-section rotation due to the shear. Moreover, $f(z)$ is a function that describes the shear theory presented in Table 1.

The strain field is given by:

$$\varepsilon_{xx} = \frac{\partial u}{\partial x} = -z \frac{\partial^2 w}{\partial x^2} + f(z) \frac{\partial \phi}{\partial x} \quad (2)$$

$$\gamma_{xz} = \left(\frac{\partial w}{\partial x} + \frac{\partial u}{\partial z} \right) = \frac{df(z)}{dz} (\phi) \quad (3)$$

Using the constitutive laws for orthotropic materials [15] is possible to obtain the stress field presented in Eq.(4) e Eq.(5):

$$\sigma_{xx} = Q_{11} \varepsilon_{xx} \quad (4)$$

$$\tau_{xz} = Q_{55} \gamma_{xz} \quad (5)$$

where

$$Q_{11} = \frac{1}{(-1 + \nu_{xy} \nu_{yx})} \begin{pmatrix} E_{xx} \cos(\theta)^4 \\ + (E_{yy} \nu_{xy} + E_{xx} \nu_{yx}) \cos(\theta)^2 \sin(\theta)^2 \\ + E_{yy} \sin[\theta]^4 \\ + G_{xy} (1 - \nu_{xy} \nu_{yx}) \sin[2\theta]^2 \end{pmatrix} \quad (6)$$

$$Q_{55} = G_{zx} \cos(\theta)^2 + G_{yz} \sin(\theta)^2. \quad (7)$$

Moreover, E_{ij} and G_{ij} ($i, j = x, y$) are longitudinal and transversal elasticity modules, respectively, concerning the principal axes; θ is the angle between the fiber and the beam's principal axis.

In free vibration analysis, the Hamilton principle [22] is used to obtain the equations of motion for the displacement field given by Eq.(1). Thus, the equations that describe the problem and its boundary conditions are presented in Eq.(8), Eq.(9) and Eq.(10), respectively.

$$A_0 \frac{\partial^4 w}{\partial x^4} - B_0 \frac{\partial^3 \phi}{\partial x^3} - \left(\rho \frac{A_0}{Q_{11}} \frac{\partial^4 w}{\partial x^2 \partial t^2} \right) + \left(\rho \frac{B_0}{Q_{11}} \frac{\partial^3 \phi}{\partial t^2 \partial x} \right) + \left(\rho b h \frac{\partial^2 w}{\partial t^2} \right) = q \quad (8)$$

$$B_0 \frac{\partial^3 w}{\partial x^3} - C_0 \frac{\partial^2 \phi}{\partial x^2} + D_0 \phi - \rho \left(\frac{B_0}{Q_{11}} \frac{\partial^3 w}{\partial x \partial t^2} - \frac{C_0}{Q_{11}} \frac{\partial^2 \phi}{\partial t^2} \right) = 0 \quad (9)$$

$$\left. \begin{array}{c} w \\ \frac{\partial w}{\partial x} \\ \phi \end{array} \right\} \text{ or } \left. \begin{array}{c} \hat{V}_x = \left[-A_0 \frac{\partial^3 w}{\partial x^3} + B_0 \frac{\partial^2 \phi}{\partial x^2} - \frac{\rho A_0}{Q_{11}} \frac{\partial^3 w}{\partial x \partial t^2} + \frac{\rho B_0}{Q_{11}} \frac{\partial^2 \phi}{\partial x^2} \right] \\ M_{xy} = \left[-A_0 \frac{\partial^2 w}{\partial x^2} + B_0 \frac{\partial \phi}{\partial x} \right] \\ \hat{M}_{xy} = \left[-B_0 \frac{\partial^2 w^{ESL}}{\partial x^2} + C_0 \frac{\partial \phi}{\partial x} \right] \end{array} \right\} \quad (10)$$

such that:

$$A_0 = \left(Q_{11} \int_A z^2 dA \right) = Q_{11} b \sum_{k=1}^N \int_{z_{k+1}}^z z^2 dz \quad (11)$$

$$B_0 = \left(Q_{11} \int_A z f(z) dA \right) = Q_{11} b \sum_{k=1}^N \int_{z_{k+1}}^z z f(z) dz \quad (12)$$

$$C_0 = \left(Q_{11} \int_A f(z)^2 dA \right) = Q_{11} b \sum_{k=1}^N \int_{z_{k+1}}^z f(z)^2 dz \quad (13)$$

$$D_0 = \left(Q_{55} \int_A f'(z)^2 dA \right) = Q_{55} b \sum_{k=1}^N \int_{z_{k+1}}^z f'(z)^2 dz \quad (14)$$

Moreover, b , h , N , ρ and q represent the cross-section's width and height, the number of layers present in the laminated beam, its mass density, and the distributed load, respectively. Furthermore, \hat{V}_x , M_{xy} , and \hat{M}_{xy} represent the high-order shear, bending moment, and high-order moment, respectively.

Table 1. Shear theory present in the displacement field.

Model	Author	$f(z)$
Model 1	Reddy [5]	$f(z) = z(1 - 4z^2/3h^2)$
Model 2	Shi -Voyiadjis [6]	$f(z) = 5z/4(1 - 4z^2/3h^2)$
Model 3	Ambartsumyan [7]	$f(z) = z/2[h^2/4 - z^2/3]$
Model 4	Touratier [8]	$f(z) = h/\pi \sin[\pi z/h]$
Model 5	Soldatos [9]	$f(z) = [z \cosh(0.5) - h \sinh(z/h)]$
Model 6	Karama et al. [10]	$f(z) = z \exp[-2(z/h)^2]$
Model 7	Akavci [11]	$f(z) = 3\pi/2[h \tanh(z/h) - z \sec^2(0.5)]$
Model 8	Thai et al. [12]	$f(z) = h \tan^{-1}(2z/h) - z$

In dynamic analysis, Eq.(8) and Eq.(9) is formulated as an eigenvalue problem to determine natural frequencies. Thus, Eq.(15) and Eq.(16) represent the periodic movement of the beam under free vibration [22]:

$$w(x,t) = W(x)e^{-i\omega t}, \quad (15)$$

$$\phi(x,t) = S(x)e^{-i\omega t}. \quad (16)$$

Where ω is the natural frequency of the transverse displacement; $W(x)$ and $S(x)$ are the transverse movement's mode shape. Imposing $q=0$ and replacing Eq.(15) and Eq.(16) in Eq.(8) and Eq.(9), one writes:

$$A_0 \frac{d^4 W}{dx^4} - B_0 \frac{d^3 S}{dx^3} + \left(\omega^2 \rho \frac{A_0}{Q_{11}} \frac{d^2 W}{dx^2} \right) - \left(\omega^2 \rho \frac{B_0}{Q_{11}} \frac{dS}{dx} \right) - (\omega^2 \rho A W) = 0 \quad (17)$$

$$B_0 \frac{d^3 W}{dx^3} - C_0 \frac{d^2 S}{dx^2} + D_0 S + \rho \left(\omega^2 \frac{B_0}{Q_{11}} \frac{\partial W}{\partial x} - \omega^2 \frac{C_0}{Q_{11}} S \right) = 0 \quad (18)$$

2.2. Shear stress

In order to circumvent the deficiency in the description of the interlaminar shear stress field, caused by the adoption of a class C^1 displacement field, in this work, the interlaminar stresses are obtained using the two-dimensional elasticity equilibrium equation given [15]:

$$\begin{aligned}
0 &= \frac{\partial \sigma_{xx}}{\partial x} + \frac{\partial \tau_{xz}}{\partial z} \\
0 &= \frac{\partial \tau_{xz}}{\partial x} + \frac{\partial \sigma_{zz}}{\partial z}
\end{aligned} \tag{19}$$

For each layer ($z_k \leq z \leq z_{k+1}$), Eq. (19) can be integrated concerning the height variable, z , to obtain the interlaminar stresses. Thus, the τ_{xz} shear stress is given by:

$$\tau_{xz} = - \int_{z_k}^z \left(\frac{\partial \sigma_{xx}}{\partial x} \right) dz + G^{(k)}, \tag{20}$$

where $G^{(k)}$ is an integration constant, which can be obtained by imposing the shear stress nullity on the upper and lower edges of the beam and imposing the interlaminar continuity condition.

3. Spectral Finite Element Method

This section discusses developing the high-order Spectral Finite Element Method applied to the equivalent layer theory (ESL) for laminated beams. In this work, Hermite's interpolation is used to describe the deflection, which depends on both the nodal deflection and its derivative. For the $\phi(x,t)$ rotation field, Lagrange's interpolation is used. Both in the Hermite and Lagrange approximations, the interpolating nodes are positioned at the zeros of Lobatto's polynomials, since this nodal positioning is shown to be quite efficient in modeling problems of the mechanics of solids [19].

3.1. Weak Formulation

From the weighting of Eq.17 and Eq.18 respectively, by $v(x,t)$ and $\psi(x,t)$, and integrating it in the $\Omega^e = (x_a, x_b)$ wing domain, the following equations are obtained:

$$\begin{aligned}
& \int_{x_a}^{x_b} \left(A_0 \frac{\partial^2 w}{\partial x^2} \frac{\partial^2 v}{\partial x^2} - B_0 \frac{\partial \phi}{\partial x} \frac{\partial^2 v}{\partial x^2} + \right. \\
& \left. \rho \left(\frac{A_0}{Q_{11}} \frac{\partial v}{\partial x} \frac{\partial^3 w}{\partial x \partial t^2} + bhv \frac{\partial^2 w}{\partial t^2} - \frac{B_0}{Q_{11}} \frac{\partial v}{\partial x} \frac{\partial^2 \phi}{\partial t^2} \right) \right) dx \\
& = \int_{x_a}^{x_b} v q + v \hat{V} \Big|_{x_a}^{x_b} - \frac{\partial v}{\partial x} M_{xy} \Big|_{x_a}^{x_b}
\end{aligned} \tag{21}$$

$$\begin{aligned}
& \int_{x_a}^{x_b} \left(-B_0 \frac{\partial^2 w}{\partial x^2} \frac{d\psi}{dx} + C_0 \frac{\partial \phi}{\partial x} \frac{\partial \psi}{\partial x} + D_0 \psi \phi + \right. \\
& \left. \rho \left(-\frac{B_0}{Q_{11}} \frac{\partial^3 w}{\partial x \partial t^2} \psi + \frac{C_0}{Q_{11}} \frac{\partial^2 \phi}{\partial t^2} \psi \right) \right) dx, \\
& = \psi \hat{M}_{xy} \Big|_{x_a}^{x_b}
\end{aligned} \tag{22}$$

where parameters $v(x,t)$ and $\psi(x,t)$ are homogeneous when essential boundary conditions (w , $\partial w / \partial x$ and ϕ) are prescribed.

3.2. Interpolations functions

Through Eq.(21) and Eq.(22), it is possible to observe the requirement to approximate w and ϕ by function with at least classes C^1 and C^0 , respectively. Thus, w and $\partial w / \partial x$ variables are approximated by Hermite's spectral polynomials of any order, while Lagrange's spectral polynomials of any order approximate ϕ .

Lagrange shape functions, for each element, are constructed by

$$\varphi_j^{(L)}(x) = \prod_{i=0, i \neq j}^{n_L-1} \frac{(x - x_i)}{(x_j - x_i)}, \quad (23)$$

where n_L is the number of Lagrange's nodes present in the element; the points x_k with $k=0, \dots, n_L-1$ represent the nodal coordinates in the element, which are determined by the approximate base. Thus, the ϕ function is approximated by

$$\phi(x, t) = \sum_{j=1}^{n_L} \phi_j(t) \varphi_j^{(L)}(x). \quad (24)$$

The ϕ_j parameters are the nodal values referring to the ϕ rotation.

Using the $\varphi_{w,i}^{(H)}(x_j) = \delta_{ij}$, $\partial \varphi_{w,i}^{(H)}(x) / \partial x \big|_{x=x_j} = 0$ and $\varphi_{\partial w / \partial x, i}^{(H)}(x_j) = 0$, $\partial \varphi_{\partial w / \partial x, i}^{(H)}(x) / \partial x \big|_{x=x_j} = \delta_{ij}$ constraints, it is possible to construct the Hermite's polynomials $\varphi_{w,i}^{(H)}$ and $\varphi_{\partial w / \partial x, i}^{(H)}$ of any order, see Eq. (25), from the Lagrange's polynomials $\varphi_i^{(L)}$, also of any order [23]. However, one emphasizes that the Lagrange's polynomial used in Eq. (25) does not necessarily have the same degree of approximation used for the rotation ϕ .

$$\begin{aligned} \varphi_{w,i}^{(H)}(x) &= \left[\varphi_i^{(L)}(x) \right]^2 \left(1 - 2 \frac{d\varphi_i^{(L)}}{dx}(x_i)(x - x_i) \right) \\ \varphi_{\partial w / \partial x, i}^{(H)}(x) &= \left[\varphi_i^{(L)}(x) \right]^2 (x - x_i) \end{aligned} \quad (25)$$

For $i=0, 1, \dots, n_H-1$, with n_H being the number of Hermite nodes and the x_i points are the elements nodal coordinates. Thus, the deflection's approximation, called by w , is described as follows (see Figure 2):

$$\begin{aligned} w(x, t) &= \sum_{j=1}^{n_H} w_j(t) \varphi_{w,j}^{(H)}(x) + \\ &\sum_{k=1}^{n_H} \widehat{w}_k(t) \varphi_{\partial w / \partial x, k}^{(H)}(x) = \sum_{i=1}^{2n_H} \bar{w}_i(t) \varphi_i^{(H)}(x) \end{aligned} \quad (26)$$

where $w_i(t)$ are the nodal values of the deflection, $\widehat{w}_i(t)$ are the nodal values of the rotation $\partial w / \partial x$ and

$$\bar{w}_i(t) = \begin{cases} w_i(t), & \text{if } i \text{ is odd} \\ \widehat{w}_i(t), & \text{if } i \text{ is even} \end{cases} \quad (27)$$

In order that the approximation gave in Eq. (24) is one degree less than the approximation in Eq. (25), it is possible to relate the Lagrange nodes (n_L) with the Hermite (n_H) nodes by

$$n_L = 2(n_H - 1) + 1 \tag{28}$$

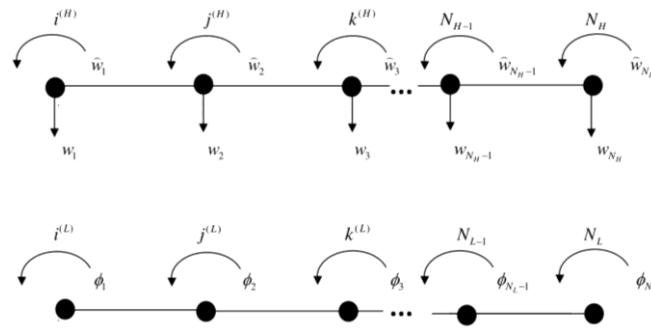


Figure 1. Interdependent interpolation for variables w , $\partial w / \partial x \mathbf{e} \phi$.

In the numerical calculation automation, regardless of size and degree of the element, the dimensionless space $-1 \leq \xi \leq 1$ is given by:

$$\xi = \frac{2}{L^e} (x - x_i) - 1, \tag{29}$$

where L^e is the element length.

This parametric mapping, see Eq. (29), for both coordinates and mechanics variables is used in SFEM for the generation of the interpolation functions.

3.3. Equidistant nodal base

The set of uniform dimensionless points $\{\xi_k \in \mathbb{R}; -1 \leq \xi_k \leq +1\}$ is obtained through [19]:

$$\xi_k = \xi_1 + r(k-1), \tag{30}$$

where $k=1, \dots, (m+1)$ is the partition of the interval $[-1, 1]$, $\xi_1 = -1$ (the starting point), $r = 2/m$ is the ratio of arithmetic progression, and m is the order of interpolation.

3.4. Lobatto's spectral base

In this work, the spectral expansions are constructed from the nodal base formed by dimensionless located in Lobatto's orthogonal polynomials' zeros. This spectral base ensures uniform convergence and prevents the appearance of the Runge phenomenon, both for the geometric approximation and for the problem's physical variables, as the approximation function's order is high [19].

The recurrence formula for Lobatto's polynomials is given by [23]:

$$L_{o_i}(\xi) = \frac{1}{\xi^2 - 1} [(i+1)\xi P_{i+1}(\xi) - (i+1)P_i(\xi)], \quad i \geq 0 \tag{31}$$

with, P_i and P_{i+1} , Legendre's polynomials described by the following recurrence formula

$$P_{i+1}(\xi) = \frac{2i+1}{i+1} \xi P_i(\xi) - \frac{i}{i+1} P_{i-1}(\xi) \tag{32}$$

where $-1 \leq \xi \leq 1$, $P_0(\xi) = 1$ and $P_1(\xi) = \xi$.

3.5. SFEM-1D formulation

The high-order spectral finite element model for a $\Omega^e = (x_a, x_b)$ domain is developed by replacing the Eq. (24) and Eq. (25) in the weak formulation (Eq. (21) and Eq. (22)) and using the Galerkin Method ($v \approx \bar{w}_i \phi_i^{(H)}$ and $\psi \approx \phi_j \phi_j^{(L)}$) to obtain Eq. (33).

$$\begin{aligned} & \begin{bmatrix} [\mathbf{K}^{11}] & [\mathbf{K}^{12}] \\ [\mathbf{K}^{21}] & [\mathbf{K}^{22}] \end{bmatrix} \begin{Bmatrix} \{\bar{\mathbf{w}}\} \\ \{\mathbf{f}\} \end{Bmatrix} + \\ & \begin{bmatrix} [\mathbf{M}^{11}] & [\mathbf{M}^{12}] \\ [\mathbf{M}^{21}] & [\mathbf{M}^{22}] \end{bmatrix} \begin{Bmatrix} \{\ddot{\bar{\mathbf{w}}}\} \\ \{\dot{\mathbf{f}}\} \end{Bmatrix} = \begin{Bmatrix} \{\mathbf{F}^1\} \\ \{\mathbf{F}^2\} \end{Bmatrix} \end{aligned} \quad (33)$$

where:

$$\begin{aligned} K_{ii}^{11} &= \int_{x_a}^{x_b} \left(A_0 \frac{d^2 \phi_i^{(H)}}{dx^2} \frac{d^2 \phi_i^{(H)}}{dx^2} \right) dx, \\ K_{ij}^{12} &= \int_{x_a}^{x_b} \left(-B_0 \frac{d^2 \phi_i^{(H)}}{dx^2} \frac{d \phi_j^{(L)}}{dx} \right) dx, \\ K_{ji}^{21} &= \int_{x_a}^{x_b} \left(-B_0 \frac{d \phi_j^{(L)}}{dx} \frac{d^2 \phi_i^{(H)}}{dx^2} \right) dx, \\ K_{jj}^{22} &= \int_{x_a}^{x_b} \left(C_0 \frac{d \phi_j^{(L)}}{dx} \frac{d \phi_j^{(L)}}{dx} + D_0 \phi_j^{(L)} \phi_j^{(L)} \right) dx \end{aligned} \quad (34)$$

$$\begin{aligned} M_{ii}^{11} &= \int_{x_a}^{x_b} \rho \left(\frac{A_0}{Q_{11}} \frac{d \phi_i^{(H)}}{dx} \frac{d \phi_i^{(H)}}{dx} + bh \phi_i^{(H)} \phi_i^{(H)} \right) dx, \\ M_{ij}^{12} &= \int_{x_a}^{x_b} \left(-\rho \frac{B_0}{Q_{11}} \frac{d \phi_i^{(H)}}{dx} \phi_j^{(L)} \right) dx, \\ M_{ji}^{21} &= \int_{x_a}^{x_b} \left(-\rho \frac{B_0}{Q_{11}} \frac{d \phi_j^{(L)}}{dx} \phi_i^{(H)} \right) dx, \\ M_{jj}^{22} &= \int_{x_a}^{x_b} \left(\rho \frac{C_0}{Q_{11}} \phi_j^{(L)} \phi_j^{(L)} \right) dx \end{aligned} \quad (35)$$

$$\begin{aligned} F_i^1 &= \int_{x_a}^{x_b} (q \phi_i^{(H)}) dx + Q_i, \quad F_j^2 = Q_j \\ Q_1 &\equiv -\widehat{V}_x(x_a), \quad Q_2 \equiv -M_{xy}(x_a), \\ Q_3 &\equiv -\widehat{V}_x(x_b), \quad Q_4 \equiv M_{xy}(x_b), \\ Q_5 &\equiv -\widehat{M}_{xy}(x_a), \quad Q_6 \equiv \widehat{M}_{xy}(x_b) \end{aligned} \quad (36)$$

4. Numerical Results

In this section, the efficiency of any order spectral finite element method coupled with the ESL theory (SFEM-ESL) is analyzed when laminated beams in static or dynamic behavior are considered.

In the static case, displacement fields (transverse and longitudinal) and stress fields (Normal and shear) for a beam subjected to a sinusoidal load (Figure 3a) is analyzed. The beam has three layers with a stacking configuration equal to $0^\circ / 90^\circ / 0^\circ$, referring to the angle that the fibers form with the beam's axis. Moderately thick beams with an $L / h = 4$ ratio were considered since, in this situation, the effects of shear are prominent concerning those of bending. In this static analysis, the results obtained by SFEM-ESL are compared with the analytical ones developed by Pagano [20].

For the static analysis, a rapidly increasing intensity for the load (Figure 3b), described by function $q(x) = L^2 / [L^2 + 25(L - 2x)^2]$, was imposed on the structure, and the deflection was analyzed. In this case, the loading function is approximated both by the equally spaced base and by the Lobatto's base.

For the dynamic analysis, the beam in Figure 3a is subjected to free vibration, with a stacking configuration equal to $0^\circ / 90^\circ / 0^\circ$ and L / h ratio varying from 100, 10, and 5. The results obtained by SFEM-ESL are compared to those obtained by the three-dimensional FEM [21].

In all examples, the graphite-epoxy material was considered, whose elasticity modulus and Poisson's coefficients are:

$$\begin{aligned} E_x = 25MPa \quad G_{xy} = 0.5MPa \quad E_y = 1MPa \\ G_{yz} = 0.2MPa \quad \nu_{xy} = \nu_{yz} = 0.25 \end{aligned} \quad (37)$$

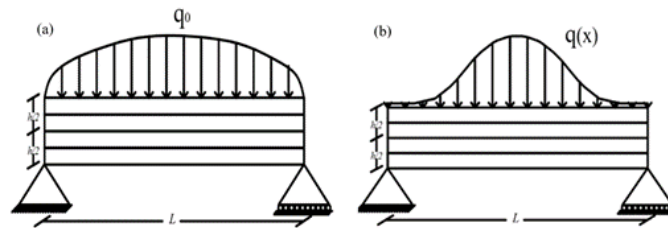


Figure 3. Simply supported beam subjected to load a) sinusoidal b) with increasing behavior.

In order to present the results independently of the geometric and loading parameters, the dimensionless response fields are written as follows:

$$\begin{aligned} \bar{u}(0, z, 0) = \frac{uE_y b}{q_0 h}, \quad \bar{w}(x, 0) = \frac{100wE_y b h^3}{q_0 L^4}, \\ \bar{\sigma}_x\left(\frac{L}{2}, z, 0\right) = \frac{b\sigma_x}{q_0}, \quad \bar{\tau}_{xz}(0, z, 0) = \frac{b\tau_{xz}}{q_0}, \\ \bar{\omega} = \omega \left(L^2 \sqrt{\frac{\rho b h}{A_0}} \right), \quad S = \frac{L}{h}, \end{aligned} \quad (38)$$

where \bar{u} is the longitudinal displacement of the cross-section, \bar{w} is the deflection, $\bar{\sigma}_x$ is the Normal stress, $\bar{\tau}_{xz}$ is the Shear stress, all of these parameters are dimensionless; Furthermore,

q_0 is the amplitude of the load and $\bar{\omega}$ is the natural frequency of the first mode of vibration. The following L_2 norm was used to calculate the relative error:

$$\text{error}_{L_2}(\%) = \frac{\sqrt{(VR_1 - VC_1)^2 + \dots + (VR_n - VC_n)^2}}{\sqrt{(VR_1)^2 + \dots + (VR_n)^2}} \times 100\% . \quad (39)$$

The VR_i and VC_i ($i=1,2,\dots,n$) terms are called reference values and calculated values, respectively.

4.1. Static Analysis

The results presented in Figure 4a - 4d were obtained through the formulation SFEM-ESL, with only a single element having five Hermite's nodes for approximate w , and nine Lagrange's nodes for function ϕ . Although the ESL theory recovers its maximum value for axial displacement, the kinematic models, coupled with the ESL theory, do not show the expected zig-zag behavior (see Figure 4a). Regarding the stresses, the ESL theory had not recovered the reference values in the interlaminar region [15]. This problem is due to the class C^1 displacement field, thus providing continuity in the shear strain field and discontinuity for the shear stress field. Therefore, to overcome this obstacle, the shear stress was obtained through the equilibrium equations of elasticity (Eq. 12), allowing continuity in the shear stress (see Figure 4d).

In Figure 5, the error in the L_2 norm for the analyzed response fields is shown. It is observed that the parabolic theories of Reddy [5], Shi-Voyiadjis [6], and Ambartsumyan [7] present the same error for stresses and displacements and differing only in the behavior of the ϕ rotation. Unlike the previous example, the ESL models by Karama et al. [10] and Thai et al. [12] present the best results. While using the Thai et al. model [12], errors of less than 20%, 12.5%, 4%, and 1% were obtained for the fields of longitudinal displacement, longitudinal stress, deflection, and shear stress, respectively. On the other hand, parabolic and trigonometric theories had errors for the same response fields above less than 32%, 21%, 6%, and 5%, respectively.

In the next example, the response fields for a simply supported beam, subjected, on the surface $z = -h/2$, to a distributed load described by the equation $q(x) = L^2 / [L^2 + 25(L - 2x)^2]$, as shown in Figure 3b, are analyzed. The beam consists of epoxy graphite, whose properties have already been presented, with stacking configuration $0^\circ/90^\circ/0^\circ$ and geometric parameters $S = 4$ and thickness $b = 1m$.

As the different cinematic results were similar in this example, only the results obtained by Reddy's theory [5] are presented for simplicity. In numerical approach was considered a single element of seven Hermite's nodes, to approximate the deflection and its derivative, and thirteen Lagrange's nodes, to approximate ϕ . The loading was modeled by a single element and approximated by Lagrange's polynomial, both at the base of Lobatto (Figure 6a) and the equally spaced base (Figure 6b). In both approaches, the degree of approximation was varied. For the reference solution, the classic SFEM is considered with twenty elements. Each element is containing two Hermite's nodes and three Lagrange's nodes to describe the domain. Still in the reference solution, the loading was approximated by twenty Lagrange's quadratic elements.

In Figure 6, the deflection is shown both considering the equally spaced base (Figure 6b) and considering the Lobatto's base (Figure 6a), as the degree of loading approach is increased. From these graphs, it is observed that the SFEM-ESL that use the equally spaced nodes

provide results that diverge from the referential and which uses the Lobatto nodes lead to convergent results. The convergence of SFEM-ESL, when using Lobatto's nodes, and divergence, when using the equally spaced base, is evidenced in the analysis of the relative error for maximum deflection, shown in Figure 7.

4.2. Free vibration analysis

In this work, the natural frequency is obtained by solving the eigenvalue problem presented in the Eq.(17) and Eq.(18), via the Spectral Finite Element Method. Thus, the approximation for the vibration modes $W(x)$ and $S(x)$ is given by:

$$W(x,t) \approx \sum_{i=1}^m W_i(t) \varphi_i^{(H)}(x), \quad S(x,t) \approx \sum_{j=1}^n S_j(t) \varphi_j^{(L)}(x), \quad (40)$$

where $\varphi_j^{(H)}$ and $\varphi_j^{(L)}$ are Hermite's and Lagrange's interpolating functions, respectively. When replacing Eq. (40) in the Eq. (17) and Eq. (18), the finite element model is developed:

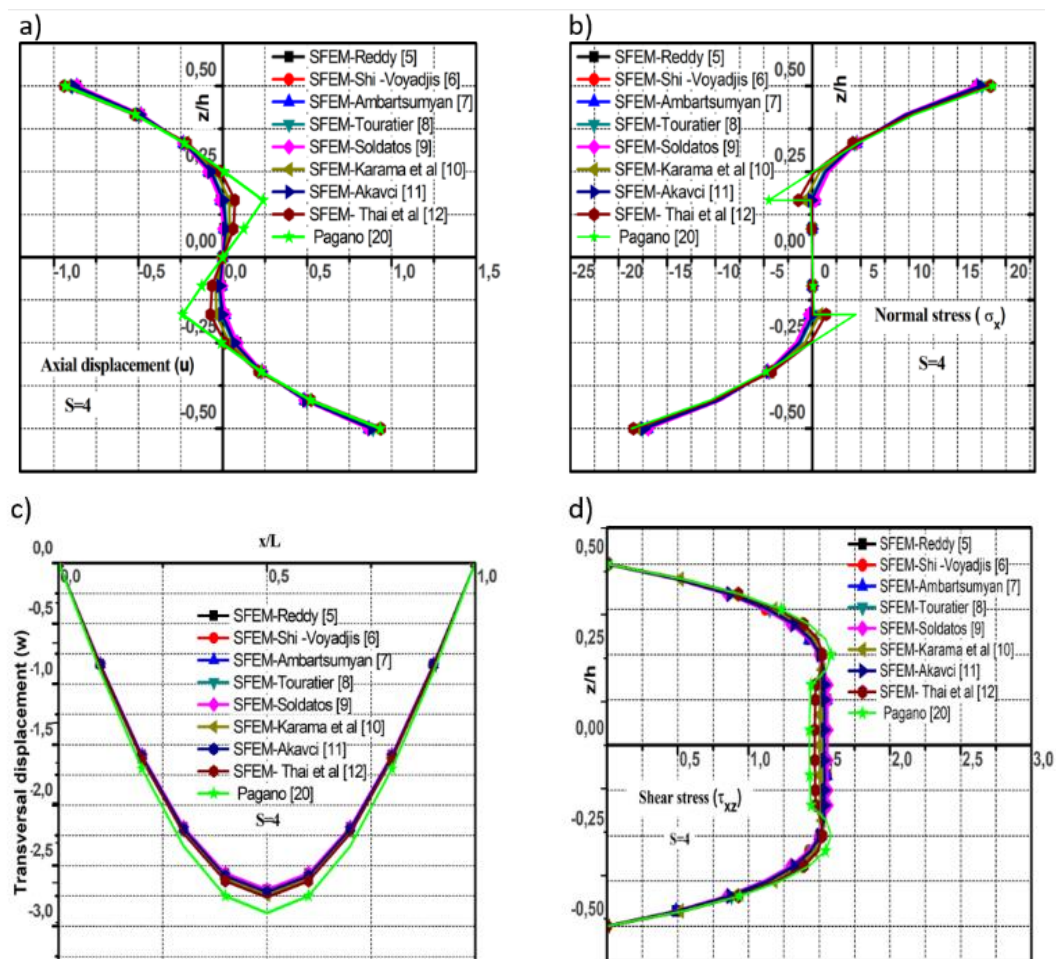


Figure 4. Description via SFEM-ESL, with 5 Hermite's nodes and with stacked layers ($0^0 / 90^0 / 0^0$), for (a) longitudinal displacement, (b) normal stress, (c) deflection along the beam, and (d) shear stress.

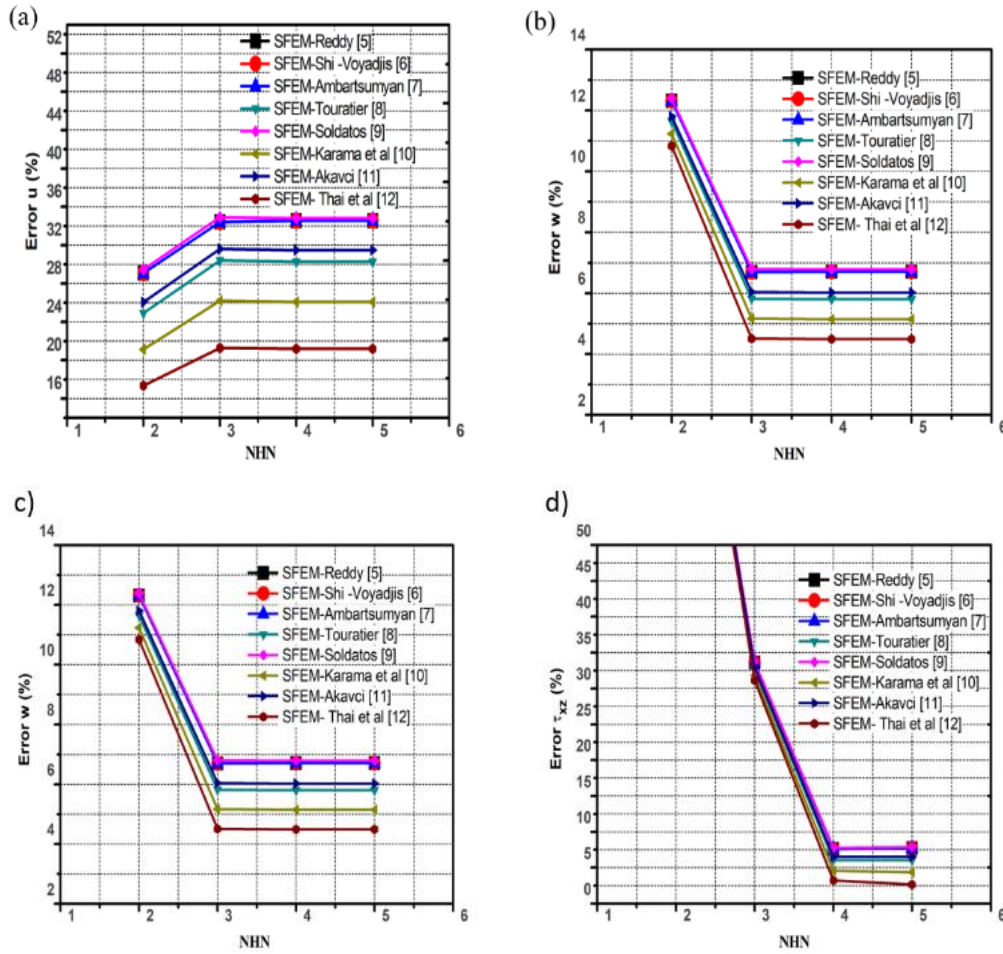


Figure 5. The relative error for a) longitudinal displacement, b) normal stress, c) deflection, and d) shear stress as the number of Hermite's nodes (NHN) is increased for laminated beam ($0^0/90^0/0^0$).

$$\begin{pmatrix} \begin{bmatrix} \mathbf{K}^{11} & \mathbf{K}^{12} \\ \mathbf{K}^{21} & \mathbf{K}^{22} \end{bmatrix} \\ \omega^2 \begin{bmatrix} \mathbf{M}^{11} & \mathbf{M}^{12} \\ \mathbf{M}^{21} & \mathbf{M}^{22} \end{bmatrix} \end{pmatrix} \begin{Bmatrix} \{\mathbf{W}\} \\ \{\mathbf{S}\} \end{Bmatrix} = \begin{Bmatrix} \mathbf{0} \\ \mathbf{0} \end{Bmatrix} \quad (41)$$

To show the efficiency of the model proposed (Eq. 41), it is considered a beam simply supported subject to free vibration, stacking configuration $0^0/90^0/0^0$, and parameter $S(=L/h)$ varying in 100, 10, and 5. A single element with three Hermite's nodes and five Lagrange's nodes were used in the discretization.

Table 2 shows the comparison between SFEM-ESL (three Hermite's nodes) and the three-dimensional numerical solution obtained in Giunta *et al.* [21] for the dimensionless natural frequency, according to Eq. (38). From Table 2, it is observed that all theories present good efficiency in obtaining natural frequency $\bar{\omega}$, with relative errors less than 4.3%. Among the models analyzed, that of Thai *et al.* [12] obtained a maximum error of less than 2.7% for all cases examined, while the parabolic theories showed maximum errors of more than 4%. Finally, it is observed that the values of natural frequency obtained by SFEM become less consistent with the reference values as the value of parameter S decreases, that is, as the beam becomes thick.

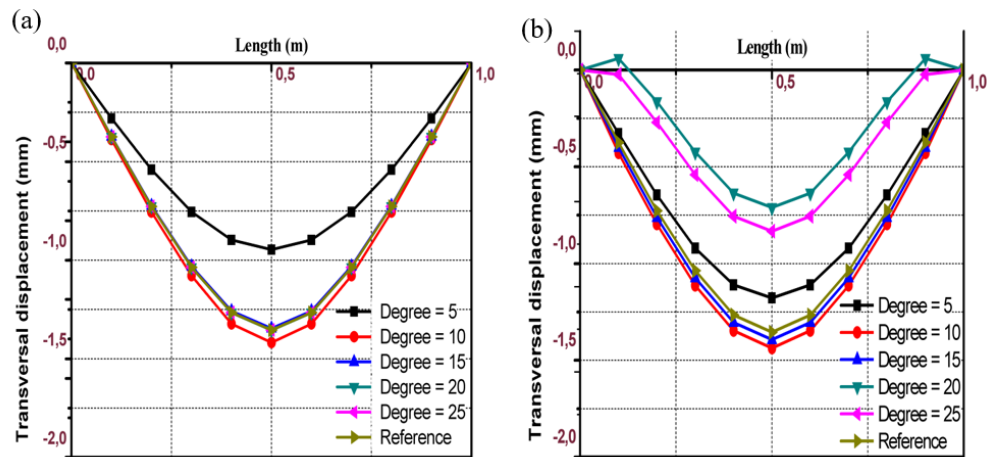


Figure 6. Deflection obtained by SFEM-ESL for laminated beam ($0^0/90^0/0^0$). Approximate loading by Lobatto's base (a) and equally spaced base (b).

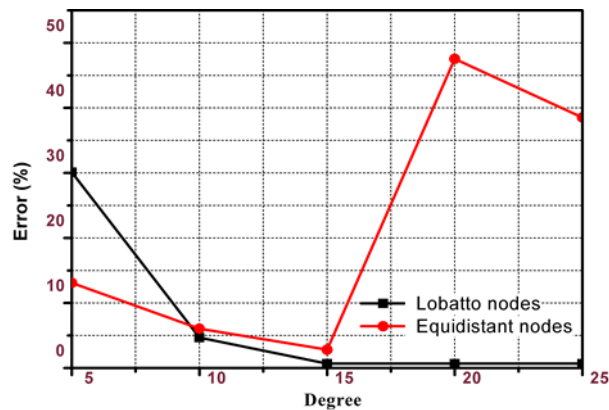


Figure 7. The relative error for maximum deflection in the laminated beam ($0^0/90^0/0^0$).

Table 2. The natural frequency $\bar{\omega}$ for ($0^0/90^0/0^0$) simply supported beam.

Author l	S=100	S=10	S=10
Reddy [5]	13,957	10,683	7,182
Shi -Voyiadjis [6]	13,957	10,683	7,182
Ambartsumyan [7]	13,957	10,683	7,182
Touratier [8]	13,956	10,636	7,142
Soldatos [9]	13,957	10,687	7,186
Karama et al. [10]	13,955	10,593	7,107
Akavci [11]	13,956	10,649	7,152
Thai et al. [12]	13,953	10,546	7,071
FEM 3D [21]	13,932	10,334	6,888

5. Conclusions

In this work, a Spectral Finite Element Model (SFEM) was developed for the unified high-order beam theories applied to the analysis of laminated beams. In the variationally consistent formulation, the governing equation and its primary and secondary boundary conditions were constructed.

In static analysis, the primary variables referring to deflection and its derivative were approximated by Hermite's polynomial, due to their dependence. Moreover, the rotation variable was approximated by Lagrange's polynomial due to its independence from the other variables. The Hermite's polynomials were constructed from the Lagrange's polynomials, according to Eq. (25). Both the Hermite and Lagrange's polynomials used the nodal points in the zeros of the Lobatto's polynomials in the spectral approach. To circumvent the shear locking problem, the degree of approximation of the rotation variable is once less than the degree of approximation for deflection.

In the dynamic approach, in addition to the static variables, the $W(x)$ and $S(x)$ vibration modes were approximated by Hermite and Lagrange's polynomials, respectively. In both approaches, nodal points (or interpolators) were used in the zeros of Lobatto's polynomials, characterizing the spectral approach.

Figure 4 and Figure 5 show that both for the displacement field and the stress field, all kinematic models decrease the error concerning the reference solution, as the approximation's degrees increase, highlighting the Thai model. It is noteworthy that the shear stress had errors of less than 5% for any model used. However, to achieve this error, the shear stress field was determined using the two-dimensional elasticity equilibrium equation. It emphasizes that longitudinal displacement (u) presents maximum values in agreement with Pagano's solution [20], in all models.

Additionally, the problem of a simply supported laminated beam subjected to a load with rapidly increasing behavior was analyzed. This problem was modeled by finite elements, with an equally spaced nodal base called FEM and Lobatto's spectral base called SFEM. It was observed in Figure 6, and Figure 7 that the FEM model diverged from the reference value as the degree of approximation of loading was varied. Conversely, results convergent to the reference ones were obtained when using the SFEM model.

Given the results presented, we can see that SFEM-ESL is significantly efficient in analyzing laminated beams, especially when beams are subjected to loads with rapidly increasing behavior.

Acknowledgments

The authors would like to acknowledge the Federal University of Sergipe, through the institutional program PIBIC, for their support in carrying out this work.

References

- [1] A. Sayyad, Y. Ghugal, Bending, buckling and free vibration of laminated composite and sandwich beams: A critical review of literature, *Composite Structures*, Vol. 171, 03/01, 2017.
- [2] K. M. Liew, Z. Z. Pan, L. W. Zhang, An overview of layerwise theories for composite laminates and structures, *Development, numerical implementation and application*, Vol. 216, pp. 240-259, 5/15, 2019.

- [3] R. K. Binia, K. Smitha, Engineering applications of laminated composites and various theories used for their response analysis, in *Proceeding of*, CRC Press, pp. 67.
- [4] S. P. Timoshenko, LXVI. On the correction for shear of the differential equation for transverse vibrations of prismatic bars, *The London, Edinburgh, and Dublin Philosophical Magazine and Journal of Science*, Vol. 41, No. 245, pp. 744-746, 1921.
- [5] J. N. Reddy, A simple higher-order theory for laminated composite plates, 1984.
- [6] G. Shi, G. Z. Voyiadjis, A sixth-order theory of shear deformable beams with variational consistent boundary conditions, *Journal of Applied Mechanics*, Vol. 78, No. 2, 2011.
- [7] S. A. Ambartsumyan, On theory of bending plates, *Izv Otd Tech Nauk AN SSSR*, Vol. 5, No. 5, 1958.
- [8] M. Touratier, An efficient standard plate theory, *International journal of engineering science*, Vol. 29, No. 8, pp. 901-916, 1991.
- [9] K. Soldatos, A transverse shear deformation theory for homogeneous monoclinic plates, *Acta Mechanica*, Vol. 94, No. 3-4, pp. 195-220, 1992.
- [10] M. Karama, K. Afaq, S. Mistou, Mechanical behaviour of laminated composite beam by the new multi-layered laminated composite structures model with transverse shear stress continuity, *International Journal of solids and structures*, Vol. 40, No. 6, pp. 1525-1546, 2003.
- [11] S. Akavci, Buckling and free vibration analysis of symmetric and antisymmetric laminated composite plates on an elastic foundation, *Journal of Reinforced Plastics and Composites*, Vol. 26, No. 18, pp. 1907-1919, 2007.
- [12] C. H. Thai, A. Ferreira, S. P. A. Bordas, T. Rabczuk, H. Nguyen-Xuan, Isogeometric analysis of laminated composite and sandwich plates using a new inverse trigonometric shear deformation theory, *European Journal of Mechanics-A/Solids*, Vol. 43, pp. 89-108, 2014.
- [13] A. S. Sayyad, Y. M. Ghugal, R. Borkar, Flexural analysis of fibrous composite beams under various mechanical loadings using refined shear deformation theories, *Composites: Mechanics, Computations, Applications: An International Journal*, Vol. 5, No. 1, 2014.
- [14] Z. Kheladi, S. M. Hamza-Cherif, M. Ghernaout, Free vibration analysis of variable stiffness laminated composite beams, *Mechanics of Advanced Materials and Structures*, pp. 1-28, 2020.
- [15] J. N. Reddy, 2003, *Mechanics of laminated composite plates and shells: theory and analysis*, CRC press,
- [16] P. Heyliger, J. Reddy, A higher order beam finite element for bending and vibration problems, *Journal of sound and vibration*, Vol. 126, No. 2, pp. 309-326, 1988.
- [17] A. Żak, M. Krawczuk, Certain numerical issues of wave propagation modelling in rods by the Spectral Finite Element Method, *Finite Elements in Analysis and Design*, Vol. 47, No. 9, pp. 1036-1046, 2011.
- [18] C. Willberg, S. Duczek, J. V. Perez, D. Schmicker, U. Gabbert, Comparison of different higher order finite element schemes for the simulation of Lamb waves, *Computer methods in applied mechanics and engineering*, Vol. 241, pp. 246-261, 2012.
- [19] L. P. R. Almeida, H. M. Souza Santana, F. C. Da Rocha, Analysis of High-order Approximations by Spectral Interpolation Applied to One-and Two-dimensional Finite Element Method, *Journal of Applied and Computational Mechanics*, Vol. 6, No. 1, pp. 145-159, 2020.
- [20] N. Pagano, Exact solutions for composite laminates in cylindrical bending, *Journal of composite materials*, Vol. 3, No. 3, pp. 398-411, 1969.

- [21] G. Giunta, F. Biscani, S. Belouettar, A. Ferreira, E. Carrera, Free vibration analysis of composite beams via refined theories, *Composites Part B: Engineering*, Vol. 44, No. 1, pp. 540-552, 2013.
- [22] J. Reddy, Energy and variational principles in applied mechanics, 1984.
- [23] C. Pozrikidis, 2005, *Introduction to finite and spectral element methods using MATLAB*, CRC Press,